


 Cite this: *New J. Chem.*, 2022, **46**, 5043

Mechanism of CO₂ hydrogenation over a Zr₁-Cu single-atom catalyst

 Lingna Liu,^{ab} Xujia Wang,^a Shuwei Lu,^a Jiawei Li,^a Hui Zhang,^a Xuanyue Su,^a Fan Xue,^{id}*^a Baowei Cao^a and Tao Fang^c

The effects of Zr single atom modification on the hydrogenation mechanism of CO₂ to methanol on the Cu(111) surface were investigated by density functional theory (DFT). In the HCOO pathway, 11 elementary steps were involved, which were analyzed from the aspects of kinetics and thermodynamics of each elementary reaction. bi-HCOO*, HCOOH*, H₂COO*, H₂COOH*, H₂CO* and H₃CO* are the key intermediates that are most likely to be generated. The elementary reactions of H₂COO*, H₂CO* and H₃CO* hydrogenation have relatively high activation barriers of about 1 eV, and they are the rate-limiting steps in this pathway. The desorption barriers of HCOOH* and H₂CO* are much higher than the energy barriers required for continued hydrogenation; therefore, the formation of by-products is inhibited on the Zr₁-Cu single atom catalyst surface. In the COOH pathway, the hydrogenation product *trans*-COOH* of CO₂ can further hydrogenate to *t,t*-COHOH* through the formation of O-H bonds; then, it facily dissociates into COH*, and COH* continues to hydrogenate into HCOH*, H₂COH* and the final product of CH₃OH. The last step is the rate-limiting step, with an activation energy of 1.48 eV. In the RWGS pathway, *trans*-COOH* transforms to *cis*-COOH*, and its continued hydrogenation is more favorable than dissociation in terms of kinetics and thermodynamics. The generated HCOOH is incorporated into the HCOO pathway. The results show that the HCOO pathway is more likely to occur and has higher selectivity on Zr-modified Cu-based catalysts.

 Received 17th December 2021,
 Accepted 4th February 2022

DOI: 10.1039/d1nj05938f

rsc.li/njc

1. Introduction

Carbon dioxide (CO₂) is an abundant and inexpensive C1 resource. Reduction and conversion of CO₂ into small organic molecules or hydrocarbons can not only alleviate global warming caused by the greenhouse effect, but also provide a new way to meet future energy demand.¹ Hydrogenation products of CO₂ mainly include methanol (CH₃OH),^{2–5} methane (CH₄),^{6,7} formic acid (HCOOH),^{8–10} dimethyl ether (CH₃OCH₃),^{11–13} and CO.^{14–18} CO is used to produce liquid fuels such as olefin and polyol through the Fischer-Tropsch (FT) process and other mature processes.^{19–24} Methanol is a liquid solar fuel, and it is highly significant to realize the hydrogenation of CO₂ to methanol.²⁵

The hydrogenation process of CO₂ to methanol is complex. The intermediate species, elemental reaction and rate-limiting steps involved vary with the catalysts and reaction conditions. The initial hydrogenation of CO₂ can generate the intermediate

formate (HCOO), by forming a C-H bond, or COOH, by forming an O-H bond. It was found with XPS and TPD methods that HCOO, which is a key intermediate in methanol synthesis, is abundant on the Cu surface.²⁶ Yang *et al.*²⁷ investigated the hydrogenation reaction of CO₂ on Cu(111) and Cu nanoparticles or in the presence of a ZnO(0001) carrier by experiments and theoretical calculations. Their results indicate that methanol is synthesized *via* the HCOO pathway on Cu(111) and Cu₂₉. The reaction intermediates involved are HCOO, dioxymethylene (H₂COO), formaldehyde (H₂CO) and methoxy (H₃CO), and the reaction rates are affected by HCOO and H₂COO hydrogenation. CO is generated *via* the reverse water-gas-shift route (RWGS). Due to the instability of the formyl group (HCO) generated from CO hydrogenation, CO is easily generated by the reverse reaction. Therefore, CO accumulates on the surface of the catalyst as a by-product without subsequent hydrogenation reactions.

The introduction of Pd, Rh, Pt and Ni enhances the interaction between the intermediate species and metal surfaces, especially the adsorption of CO and HCO, promoting the formation of methanol *via* the RWGS pathway. The hydrogenation of CO₂ to carboxylate (COOH), which is then decomposed into CO and OH, and CO hydrogenation to HCO and H₂CO in turn, follows the same elemental reaction in the HCOO path.²⁸ Grabow and Mavrikakis²⁹ used DFT (GGA-PW91) calculations and micro-

^a Shaanxi Key Laboratory of Low Metamorphic Coal Clean Utilization, School of Chemistry and Chemical Engineering, Yulin University, Yulin 719000, P. R. China. E-mail: xuefan@yulinu.edu.cn; Tel: +18792919669

^b National Coal and Salt Chemical Product Quality Supervision and Inspection Center (Yulin), Yulin 719000, P. R. China

^c Department of Chemical Engineering, School of Chemical Engineering and Technology, Xi'an Jiaotong University, Xi'an 710049, P. R. China

dynamics to investigate the reaction mechanism of the hydrogenation of CO and CO₂ to methanol on the traditional commercial catalysts Cu/ZnO/Al₂O₃. They found that hydrogenation of the HCOO group is more conducive to the formation of HCOOH species than hydrogenation of the H₂COO group. HCOOH can continue hydrogenation to generate H₂COOH, and then the C–OH bond breaks to generate H₂CO. Under industrial conditions, CH₃OH is mainly obtained by hydrogenation of CO₂. When the concentration of CO₂ is low, the reaction rate is controlled by H₃CO formation. In contrast, H₃CO hydrogenation controls the reaction rate.

Kattel *et al.*,³⁰ using DFT and KMC simulations combined with DRIFTS and steady-state flow reaction tests, found that titanium dioxide and zirconium dioxide can promote methanol synthesis on Cu *via* the RWGS pathway, while the HCOO intermediate acts as a bystander. The higher activity of ZrO₂ is associated with the synergistic effect between Zr³⁺ and Cu formed at the interface, which can appropriately enhance the adsorption of CO₂, CO, HCO and H₂CO, not only promoted the occurrence of RWGS pathway but also prevented the poisoning of the active site. This not only promoted methanol synthesis *via* the RWGS pathway but also prevented the poisoning of the active sites. However, Larmier *et al.*³¹ studied the hydrogenation of CO to methanol over Cu/ZrO₂ by kinetics, FTIR and NMR analyses combined with isotope labeling and DFT calculations. They found that HCOO is the key intermediate species in the reaction process. Austin *et al.*³² constructed copper nanoparticles containing 55 copper atoms. By zirconium atom modification, they found that Zr-modified Cu nanoparticles not only have a chemisorption effect on CO₂ but also have a strong activation effect on CO₂. Compared with Cu₅₅, Cu₅₄Zr is more efficient for the dissociation of CO₂ to CO. The doping of single atom Zr has excellent catalytic activity for the reduction of CO₂ to methanol, increasing the adsorption stability of CO₂, CHO and CO, facilitating the dissociation of H₂, and reducing the energy barrier for the generation of HCO.³³ Based on d-band center and chemical hardness analysis, it was found that the adsorption energy of CO₂ could be changed through adjusting the ratio of Zr atoms in the Cu–Zr bimetallic clusters, and the adsorption stability of CO₂ was enhanced by the growth of Zr atoms.³⁴

To further clarify the reaction mechanism of CH₃OH synthesis by CO₂ hydrogenation on the surface of a Zr–Cu catalyst, the Zr-single atom-doped Cu(111) surface was chosen as the catalyst in this work. The adsorption stability of the reactants, products and intermediates was studied by DFT theoretical calculations to obtain the basic kinetic and thermodynamic data of the elementary reactions in the HCOO, RWGS and COOH pathways. By comparing the activation energy of each elementary step and pathway, the most preferable pathway for hydrogenation of CO₂ to methanol was obtained.

2. Computational details

The DMol³ module^{35,36} in the Materials Studio software package (Accelrys Inc.) was used in this study. The valence electron wave

function was expanded by the double numerical basis plus polarization (DNP) base group.³⁷ The effective nuclear potential (ECP) was used to freeze and replace the internal electrons of the metal atoms.³⁷ The Perdew–Burke–Ernzerhof (PBE) exchange correlation function was calculated using the generalized gradient approximation (GGA).^{38,39} The Brillouin integral Monkhorst–Pack grid parameter was set as $3 \times 3 \times 1$.⁴⁰ Smearing was set to 0.002 Hartree. The convergence tolerances of the energy, maximum force and displacement were set as 2×10^{-5} Hartree, 4×10^{-3} Hartree Å⁻¹ and 5×10^{-3} Å, respectively. The transition states were calculated using the complete linear synchronous transit/quadratic synchronous transit (LST/QST).⁴¹ The convergence criterion was set as 0.01 eV Å⁻¹ for the root mean square force on the atom. In addition, the rationality of the transition state structure was confirmed by frequency analysis, and the corresponding vibration mode should connect the required reactants and products.

CuZr bimetallic catalysts have been synthesized for CO₂ adsorption and activation in previous experiments. The results of energy dispersive X-ray spectroscopy showed small particles composed of Cu and Zr. The adsorption and activation of CO₂ are strongly enhanced by Zr-doped Cu catalysts. Based on these experiments, we chose Zr-single atom-doped Cu(111) as the catalyst model in this study.⁴² The bond lengths of CH₃OH molecules in the gas phase were calculated, and the corresponding values were C–O = 1.425 Å, C–H = 1.096 Å, and O–H = 0.969 Å, consistent with the previously observed experimental values of 1.43 Å, 1.09 Å and 0.95 Å, respectively.⁴³ The lattice constant of Cu(111) in this study was 3.61 Å, which was close to the experimental value of 3.62 Å.⁴³

On the surface of Cu(111), CO₂ activation plays a key role in the hydrogenation of CO₂ to methanol. The experimental results show that the formation of Zr-doped Cu-based catalysts can be promoted by the synergistic effect. In order to explore the reaction mechanism, the surface was constructed with a four-layer slab of a $p(3 \times 3)$ unit cell to model the Zr₁–Cu surface (Fig. 1), and a vacuum layer thickness of 15 Å was used to separate the supercells. The adsorption species were relaxed with the top two layers of the slab, and the bottom two atomic layers were fixed.

The activation energy (E_a) and reaction energy (ΔE) on the Zr₁–Cu surface were calculated as follows:

$$E_a = E_{TS} - E_{IS}$$

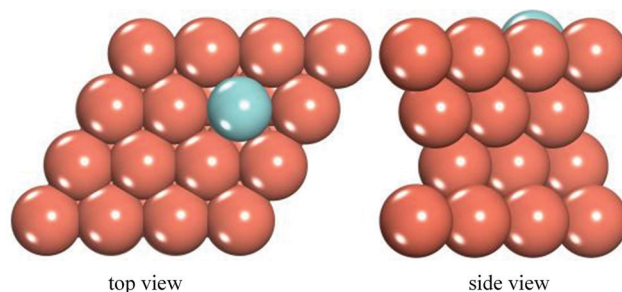


Fig. 1 Top and side views of the Zr₁–Cu surface (Cu: yellow, Zr: blue).

$$\Delta E = E_{\text{FS}} - E_{\text{IS}}$$

where E_{IS} , E_{TS} and E_{FS} denote the total energies of the initial state (IS), the transition state (TS), and the final state (FS), respectively.

3. Results and discussion

HCOO, COOH and RWGS + CO-Hydro are the three reaction pathways for the hydrogenation of CO_2 to CH_3OH . The initial and final states involved in the elementary step are the most stable adsorption configurations, as depicted in Fig. 2, 4 and 6. The activation energies and reaction energies involved are listed in Tables 1–3.

3.1 HCOO pathway

For H_2 dissociation, the initial state of H_2^* is located above the Zr atom, and the distance between Zr and H_2 is 2.298 Å. The H–H bond length of 0.775 Å is fractured by TS1-1, and the two H atoms in the final state are adsorbed at the Zr–Cu interface by the H–Zr bond. The energy barrier of this step is 0.64 eV on the Zr_1 –Cu surface, which is thermally neutral.

Geometrical parameters such as the bond length of the C–O bonds and the bond angle of CO_2 have been used to identify CO_2 activation.^{44,45} The formation of the bent structure of CO_2 is the initial step in the photoreduction.⁴⁶ CO_2^* prefers to adsorb at the bridge site on the Zr_1 –Cu surface with an

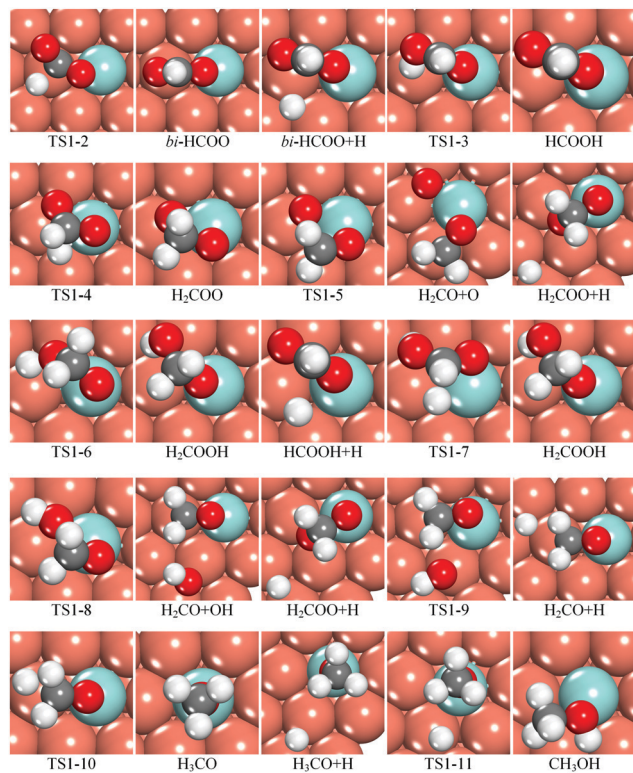


Fig. 2 Most stable adsorption configurations of the key intermediates involved in the HCOO pathway on the Zr_1 –Cu surface. H, C and O atoms are represented as white, gray, and red spheres, respectively.

Table 1 Elementary reactions involved in the HCOO pathway on the Zr_1 –Cu surface together with the activation energies (E_a /eV) and reaction energies (ΔE /eV)

No.	Elementary step	E_a	ΔE
R1-1	$\text{H}_2^* \rightarrow \text{H}^* + \text{H}^*$	0.64	–0.08
R1-2	$\text{CO}_2^* + \text{H}^* \rightarrow \text{bi-HCOO}^*$	0.60	–0.86
R1-3	$\text{bi-HCOO}^* + \text{H}^* \rightarrow \text{HCOOH}^*$	0.79	0.33
R1-4	$\text{bi-HCOO}^* + \text{H}^* \rightarrow \text{H}_2\text{COO}^*$	0.80	–0.32
R1-5	$\text{H}_2\text{COO}^* \rightarrow \text{H}_2\text{CO}^* + \text{O}^*$	0.75	–0.53
R1-6	$\text{H}_2\text{COO}^* + \text{H}^* \rightarrow \text{H}_2\text{COOH}^*$	1.04	–0.07
R1-7	$\text{HCOOH}^* + \text{H}^* \rightarrow \text{H}_2\text{COOH}^*$	0.96	–0.51
R1-8	$\text{H}_2\text{COOH}^* \rightarrow \text{H}_2\text{CO}^* + \text{OH}^*$	0.80	–0.61
R1-9	$\text{H}_2\text{COO}^* + \text{H}^* \rightarrow \text{H}_2\text{CO}^* + \text{OH}^*$	1.46	0.39
R1-10	$\text{H}_2\text{CO}^* + \text{H}^* \rightarrow \text{H}_3\text{CO}^*$	1.12	–0.78
R1-11	$\text{H}_3\text{CO}^* + \text{H}^* \rightarrow \text{CH}_3\text{OH}^*$	1.08	0.49

Table 2 Elementary reactions involved in the COOH pathway on the Zr_1 –Cu surface together with the activation energies (E_a /eV) and reaction energies (ΔE /eV)

No.	Elementary step	E_a	ΔE
R2-1	$\text{CO}_2^* + \text{H}^* \rightarrow \text{trans-COOH}^*$	0.63	–0.19
R2-2	$\text{trans-COOH}^* + \text{H}^* \rightarrow \text{t,t-COHOH}^*$	1.41	0.89
R2-3	$\text{t,t-COHOH}^* \rightarrow \text{COH}^* + \text{OH}^*$	0.68	–1.28
R2-4	$\text{t,t-COHOH}^* \rightarrow \text{t,c-COHOH}^*$	0.53	0.09
R2-5	$\text{t,c-COHOH}^* \rightarrow \text{c,c-COHOH}^*$	0.67	0.60
R2-6	$\text{c,c-COHOH}^* \rightarrow \text{COH}^* + \text{OH}^*$	0.83	–0.09
R2-7	$\text{COH}^* + \text{H}^* \rightarrow \text{HCOH}^*$	0.45	–0.28
R2-8	$\text{HCOH}^* + \text{H}^* \rightarrow \text{CH}_2\text{OH}^*$	0.43	–0.28
R2-9	$\text{H}_2\text{COH}^* + \text{H}^* \rightarrow \text{CH}_3\text{OH}^*$	1.48	–0.51

Table 3 Elementary reactions involved in the RWGS + CO-Hydro pathway on the Zr_1 –Cu surface together with the activation energies (E_a /eV) and reaction energies (ΔE /eV)

No.	Elementary step	E_a	ΔE
R3-1	$\text{trans-COOH}^* \rightarrow \text{cis-COOH}^*$	0.84	0.24
R3-2	$\text{trans-COOH}^* + \text{H}^* \rightarrow \text{HCOOH}^*$	0.94	–0.04
R3-3	$\text{cis-COOH}^* + \text{H}^* \rightarrow \text{HCOOH}^*$	0.52	–0.38
R3-4	$\text{cis-COOH}^* \rightarrow \text{CO}^* + \text{OH}^*$	1.42	0.85
R3-5	$\text{CO}^* + \text{H}^* \rightarrow \text{COH}^*$	1.57	0.65
R3-6	$\text{CO}^* + \text{H}^* \rightarrow \text{HCO}^*$	1.24	–0.58
R3-7	$\text{HCO}^* + \text{H}^* \rightarrow \text{H}_2\text{CO}^*$	0.63	–0.90
R3-8	$\text{HCO}^* + \text{H}^* \rightarrow \text{HCOH}^*$	0.78	–0.75
R3-9	$\text{H}_2\text{CO}^* + \text{H}^* \rightarrow \text{CH}_2\text{OH}^*$	1.12	0.71
R3-10	$\text{O}^* + \text{H}^* \rightarrow \text{OH}^*$	1.64	–0.68
R3-11	$\text{H}^* + \text{OH}^* \rightarrow \text{H}_2\text{O}^*$	1.28	0.79

adsorption energy of -1.35 eV, consistent with the previous DFT and experimental results of -1.29 and 1.23 eV, respectively.^{42,47} The Zr–C, Cu–C and Zr–O bond lengths of the adsorbed CO_2^* are 2.456, 2.097 and 2.111 Å, respectively. A bent configuration of CO_2 adsorption was found by a decrease in the O–C–O bond angle from 180° to 127.772° , in good agreement with the previously reported value of 126° .⁴² The calculation results indicate that the substitution of Zr atom has a positive effect on CO_2 activation.

H^* atom attacks C in CO_2 to form bi-HCOO*. In the initial structure of CO_2^*/H^* , CO_2 adsorbs on the Zr_1 –Cu surface by an O–Zr bond, where the bond angle of O=C=O is 172.216° (Fig. 2).

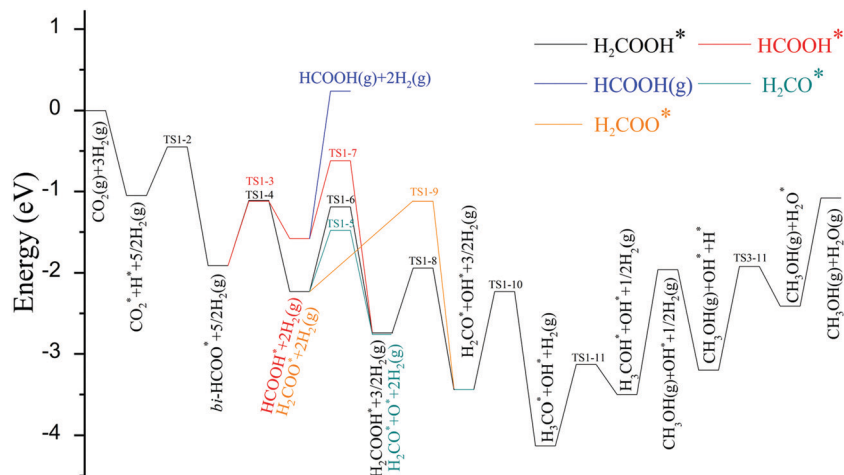


Fig. 3 Potential energy profiles of the HCOO pathway in the process of methanol synthesis from CO_2 hydrogenation on the $\text{Zr}_1\text{-Cu}$ surface.

H^* locates at the top site, and the distance between C and H^* is 2.611 Å. In TS1-2, C and H^* are close to each other, and the distance is shortened to 1.771 Å. An activation barrier of 0.60 eV must be overcome, and the heat released is 0.86 eV.

bi-HCOO* hydrogenation can form HCOOH* and H_2COO^* . In the initial state, bi-HCOO* adsorbs on the $\text{Zr}_1\text{-Cu}$ surface by Zr-O bonds, and H^* binds on the hollow sites of Cu atoms with a distance between O and H^* of 2.986 Å. In TS1-3, the H-Cu bond cleaves, and the length of the O-H bond is shortened to 1.544 Å. The activation energy of HCOOH* formation is 0.79 eV on the $\text{Zr}_1\text{-Cu}$ surface, with a reaction heat of 0.33 eV. In TS1-4, H^* approaches bi-HCOO*, and the distance between H^* and C is 1.646 Å. The activation energy of H_2COO^* formation is 0.80 eV, and the exothermic heat is 0.32 eV; then, a new C-H bond is formed in the final state. By contrast, the O-H bond is almost as difficult to form as the C-H bond (Fig. 3). The activation energy of dissociation of H_2COO^* to H_2CO^* and O^* via TS1-5 is 0.75 eV. The following step of O^* hydrogenation is as high as 1.64 eV; thus, it is difficult for this step to occur.

H_2COOH^* is the product of HCOOH* and H_2COO^* hydrogenation. H_2COO^* and H^* co-adsorb, and the distance between O and H^* is 2.881 Å in the initial state. In TS1-6, the distance between H^* and O is shortened to 1.343 Å by overcoming an energy barrier of 1.04 eV with a reaction heat of -0.07 eV. HCOOH* and H^* co-adsorb on the top site of Zr and the bridge site of Cu near Zr in the initial state, respectively. In TS1-7, the distance between the C atom in HCOOH* and H^* is reduced to 1.854 Å, and a C-H bond is formed with a bond length of 1.100 Å in the final state. A reaction heat of 0.53 eV is released. The activation barrier of C-H bond formation is similar to that of O-H bond formation (Fig. 3).

H_2COOH^* can be further dissociated into H_2CO^* to form OH^* . In TS1-8, the C-O bond cleaves and the distance between C and O increases from 1.403 Å to 3.919 Å. OH^* adsorbs on the $\text{Zr}_1\text{-Cu}$ surface through an O-Zr bond. This process overcomes the energy barrier of 0.80 eV with a large exothermic reaction energy of 0.61 eV. H_2COO^* adsorbs on the $\text{Zr}_1\text{-Cu}$ surface by an O-Zr bond in the initial state. H^* and O are close to each other when the C-O bond breaks through TS1-9. Compared with

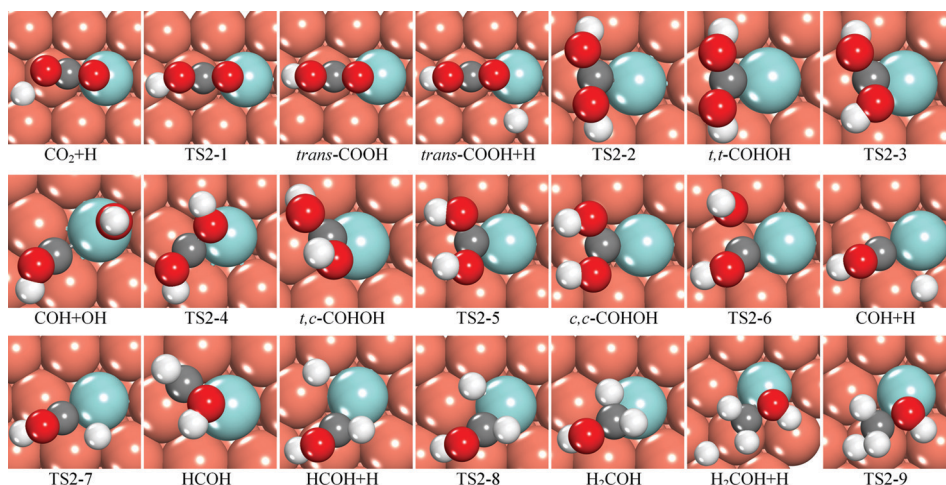


Fig. 4 Optimized structures of the intermediates in the COOH pathway of methanol synthesis from CO_2 hydrogenation on the $\text{Zr}_1\text{-Cu}$ surface.

direct dissociation of H_2COOH^* , it is obvious that this reaction is inhibited due to the very high activation barrier of 1.46 eV and endothermic reaction energy of 0.39 eV (Fig. 3).

Subsequently, H_3CO^* is produced *via* H_2CO^* hydrogenation. In the initial state, H_2CO^* adsorbs on the bridge site by C–Zr and C–Cu bonds on the $\text{Zr}_1\text{–Cu}$ surface; this is the most stable co-adsorption structure of $\text{H}_2\text{CO}^*/\text{H}^*$, where the distance between H^* and C is 2.731 Å. In TS1-10, the distance between H^* and C is shortened to 2.045 Å. The reaction is activated by the highest energy barrier of 1.12 eV in this path and releases a large heat of 0.78 eV.

H_3COH^* is formed by hydrogenation of H_3CO^* , which is the last step of the CO_2 hydrogenation reaction. For the initial $\text{H}_3\text{CO}^*/\text{H}^*$, H_3CO^* adsorbs at the top site by its O atom, while H^* binds at the hollow site. However, in TS1-11, H_3CO^* tends to occupy the top site of the Zr atom through O, while H^* locates at the top site of Cu adjacent to the Zr atom. The reaction is not facile due to the endothermic energy of 0.49 eV and the substantial energy barrier of 1.08 eV, which is 0.23 eV lower than that found in prior DFT results.⁴⁸

3.2 COOH pathway

The O–H bond can also be formed by CO_2 hydrogenation to obtain *trans*- COOH^* . In the initial state, the distances between H^* , O and C are 2.700 Å, 3.798 Å and 2.715 Å on the $\text{Zr}_1\text{–Cu}$ surface, respectively. In TS2-1 (Fig. 4), the distance between H^* and O is shortened to 2.227 Å, and CO_2^* adsorbs on $\text{Zr}_1\text{–Cu}$ surface *via* Zr–C and Zr–O bonds. The O–H bond forms with a bond length of 0.996 Å in the final state. The reaction requires an activation energy of 0.63 eV and releases heat of 0.19 eV.

H^* attacks O of *trans*- COOH^* to obtain *t,t*- COHOH^* . *trans*- COOH^*/H^* co-adsorbs on the $\text{Zr}_1\text{–Cu}$ surface in the initial state, and the length of the Zr–O bond is 2.15 Å. In TS2-2, the Zr–O bond fractures and the distance between *trans*- COOH^* and H^* decreases to 1.917 Å. The formation of *t,t*- COHOH^* is kinetically and thermodynamically inhibited due to the high activation energy barrier of 1.41 eV and reaction heat of 0.89 eV (Fig. 5). Its final state is similar to the transition state, and it forms an O–H bond with a bond length of 0.987 Å. When the elemental step takes place on the $\text{Zr}_1\text{–Cu}$ surface, there are three isomers of

COHOH^* , which are *t,t*- COHOH^* , *t,c*- COHOH^* , and *c,c*- COHOH^* . The *t,t*- $\text{COHOH}^* \rightarrow t,c$ - COHOH^* reaction overcomes the energy barrier of 0.53 eV, and this step is thermally neutral. The activation energy of *t,c*- $\text{COHOH}^* \rightarrow c,c$ - COHOH^* is 0.67 eV, and the reaction energy is 0.60 eV. Then, *c,c*- COHOH^* decomposes into OH^* and COH^* . In TS2-6, OH^* breaks away from *c,c*- COHOH^* by the cleavage of the C–O bond. COH^* adsorbs on the $\text{Zr}_1\text{–Cu}$ surface *via* a C–Cu bond and C–Zr bond, while OH^* occupies the bridge site *via* an O–Cu bond. It is thermally neutral (–0.09 eV), with an activation energy of 0.83 eV.

The product of COH^* hydrogenation is HCOH^* . H^* locates at the bridge site, and COH^* adsorbs on Zr and Cu atoms in the initial state, where the distance between C and H^* is 2.519 Å. In TS2-8, H^* bonds with Zr on the $\text{Zr}_1\text{–Cu}$ surface and gradually approaches C, by which the length is decreased to 1.759 Å. HCOH^* adsorbs on the $\text{Zr}_1\text{–Cu}$ surface at the hollow site *via* C atom in the final state. The activation energy of the reaction is 0.45 eV, and the exothermic energy is 0.28 eV.

HCOH^* is consecutively hydrogenated to form H_2COH^* . In the initial configuration of HCOH^*/H^* , HCOH^* locates near Zr and H^* adsorbs at the bridge site on the $\text{Zr}_1\text{–Cu}$ surface. The distance between C and H^* is 2.713 Å. In TS2-8, H^* and HCOH^* are close to each other, and the distance between C and H^* is shortened to 1.939 Å. In the final state, the length of the C–H bond is 1.183 Å, and the reaction activation energy is 0.43 eV, giving off a heat of 0.28 eV. The final product is obtained by H_2COH^* hydrogenation. H^* adsorbs at the hollow site and H_2COH^* occupies the Zr atom in the initial state. In TS2-9, H^* is close to H_2COH^* , and the distance between C and H^* is 1.755 Å. The reaction heat was calculated to be –0.51 eV in the COOH path with a very high energy barrier of 1.48 eV, which is 0.54 eV higher than that on Pd–Cu catalyst.⁴⁹ The calculated results indicated that the formation of the C–H bond is kinetically unfavorable (Fig. 5).

3.3 RWGS + CO-Hydro pathway

Trans- COOH^* isomerizes into *cis*- COOH^* and the direction of the H atom changes in TS3-1 (Fig. 6). The energy barrier and the reaction heat are 0.84 eV and 0.24 eV, respectively. Both *trans*-

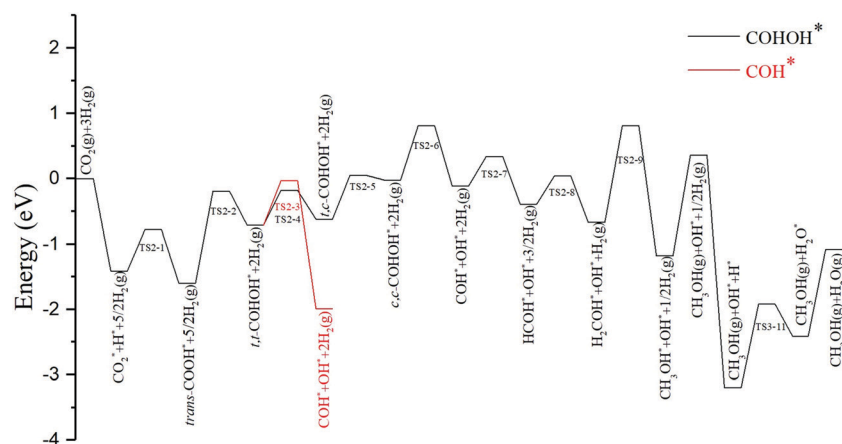


Fig. 5 Potential energy profiles of the COOH pathway in the process of methanol synthesis from CO_2 hydrogenation on the $\text{Zr}_1\text{–Cu}$ surface.

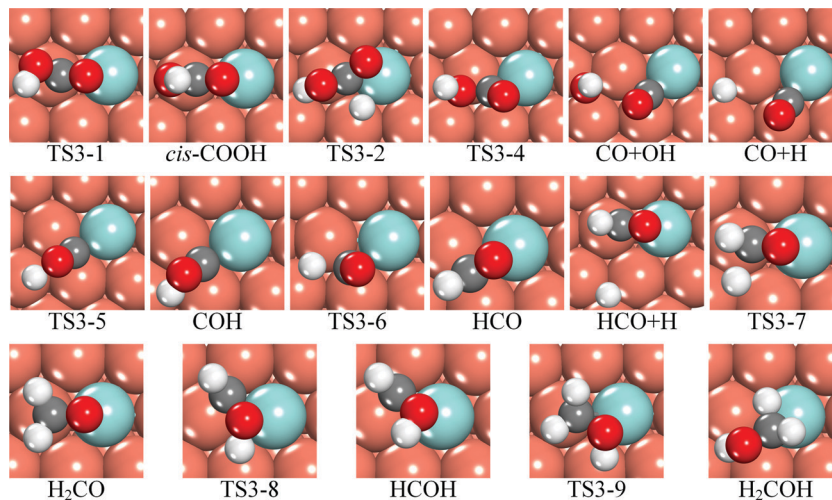


Fig. 6 Optimized structures of the intermediates in the RWGS + CO-Hydro pathway of methanol synthesis from CO₂ hydrogenation on the Zr₁-Cu surface.

COOH* and *cis*-COOH* hydrogenation can form HCOOH*. The corresponding energy barriers required are 0.94 and 0.52 eV, which are exothermic by -0.04 and -0.38 eV, respectively. HCOOH* adsorbs at the top site *via* an O-Zr bond with an adsorption energy of -1.82 eV. In addition, HCOOH* can be formed from bi-HCOO* hydrogenation in the HCOO pathway. Compared to the desorption barriers of HCOOH*, the subsequent hydrogenation is facilitated over desorption on the Zr₁-Cu surface, indicating that the production of HCOOH is suppressed.

cis-COOH* dissociates into OH* and CO*. The C-O bond length is 1.334 Å in the initial state, which is extended to 1.446 Å by TS3-4. In the final state, OH* adsorbs on the Zr₁-Cu surface at the hollow site, and the reaction overcomes an extremely high energy barrier of 1.42 eV and has a very high endothermic energy of 0.85 eV (Fig. 7). Compared to the desorption barriers of CO* (-1.57 eV), CO* hydrogenation is easier than desorption on the Zr₁-Cu surface, indicating that the production of CO is suppressed.

CO* hydrogenation can generate HCO* and COH*. In the initial state of CO*/H*, the most stable structure of CO* is

located at the top site of Zr, and H* is stable at the hollow site on the Zr₁-Cu surface. At TS3-6, the bond angle of O-C-Zr changes from 168.444° to 107.320° . In the final state, C bonds with H* to form HCO* and then adsorbs on the Zr₁-Cu surface, which requires an energy barrier of 1.24 eV and an exothermic heat of 0.58 eV. In TS3-5, CO* adsorbs stably on Zr and its adjacent Cu, and the distance between O and H* is shortened to 2.487 Å. The substantial energy barrier of COH* is calculated to be 1.57 eV, with a reaction heat of 0.65 eV.

The HCO* species undergoes continuous hydrogenation reactions to form H₂CO* and HCOH*. In the initial configuration of HCO*/H*, HCO* adsorbs at the bridge site on the Zr₁-Cu surface, and the distance between C and H* is 3.406 Å. At TS3-7, H* gradually approaches C with a length of C-H bond of 2.064 Å. In the final state, the H-C bond forms to generate H₂CO*, which can also be produced by the decomposition of H₂COO* and H₂COOH* in the HCOO route. It adsorbs at the bridge site through C-Cu and O-Zr bonds, with a calculated adsorption energy of -2.68 eV. This step gives off heat of 0.90 eV, with an activation energy of 0.63 eV. For HCOH* formation (TS3-8), the

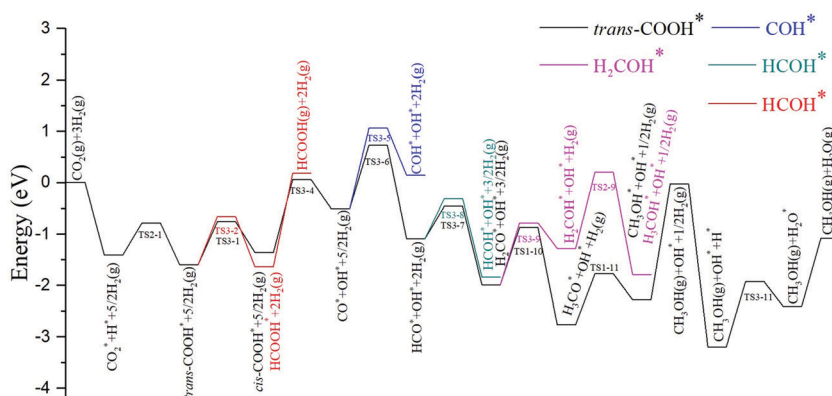


Fig. 7 Potential energy profiles of the RWGS + CO-Hydro pathway in the process of methanol synthesis from CO₂ hydrogenation on the Zr₁-Cu surface.

activation barrier is slightly higher than that of C–H bond formation (Fig. 7).

H₂CO* may be hydrogenated to H₂COH*. In the initial state, H₂CO* adsorbs on Zr and its adjacent Cu on the Zr₁–Cu surface, and H* stably occupies the hollow site of Cu. At TS3-9, O and H* are close to each other, and the final H₂COH* forms an O–H bond with a bond length of 0.985 Å. The activation energy was calculated to be 1.21 eV, and the endothermic energy is 0.71 eV. The calculated results show that H₂CO* hydrogenation is easier than desorption on the Zr₁–Cu surface.

H₂COO* can be decomposed into H₂CO* and O* groups, which subsequently produce OH* species. The initial state of O*/H* co-adsorbs at the adjacent hollow sites on the Zr₁–Cu surface. In TS3-10, H* occupies the top site, and the distance between the H* and O atoms is reduced to 1.702 Å. The bond length of O–H is 0.963 Å in the final state. The step is exothermic (–0.68 eV), with an extremely high reaction energy barrier of 1.64 eV. OH* can generate H₂O* through further reaction with the adsorbed H*. In the initial state, OH* binds at the top site and H* binds at the bridge site on the Zr₁–Cu surface. At TS3-11, H* attacks the O atom of the OH* intermediate and adsorbs at the top site. The distance between O and H* atoms decreases from 3.878 Å to 1.326 Å. Subsequently, H₂O* binds at the top site on the Zr₁–Cu surface, which is highly endothermic (0.79 eV) and has an energy barrier of 1.28 eV.

As discussed above, methanol is produced by the lowest energy HCOO pathway, which involves the intermediates of bi-HCOO*, HCOOH*, H₂COO*, H₂COOH*, H₂CO* and H₃CO*. The adsorption energies of bi-HCOO* and H₃CO* are –4.64 and –5.01 eV, respectively. In experiments, it has been observed that bi-HCOO* strongly binds and forms large amounts of H₃CO* on zirconia-supported copper even after evacuation under high vacuum.³¹ This work provides a bridge between experiment and theory, which paves the road to designing efficient catalysts for CO₂ hydrogenation.

4. Conclusions

In this research, the mechanism of hydrogenation of CO₂ to methanol over a single-atom Zr-doped Cu-based catalyst has been systematically explored by DFT calculations. Three possible paths of CO₂ + H₂ → CH₃OH are discussed. Along the HCOO pathway, the most likely elementary reactions are CO₂* → bi-HCOO* → HCOOH* (H₂COO*) → H₂CO* → H₃CO* → H₃COH*. The rate-limiting step for the reaction is H₂COO*, H₃CO* and H₂CO* hydrogenation, for which the activation energies are all about 1 eV. The desorption energies of HCOOH* and H₂CO* are higher than the activation energy of continued hydrogenation; therefore, no by-products are formed in this path. In the COOH pathway, COH* is easily dissociated through *t,t*-COOH* to generate COH*, and COH* continues to hydrogenate to generate HCOH*, H₂COH* and the final product CH₃OH. The rate-limiting step in the reaction process is H₂COH* hydrogenation, for which the activation energy is 1.48 eV. In the RWGS path, *cis*-COOH*

dissociation needs to overcome an energy barrier of 1.42 eV, while its hydrogenation only needs an energy of 0.52 eV. Therefore, this path preferably generates HCOOH* through the hydrogenation of *cis*-COOH* and merges with the HCOO path. The results show that the HCOO pathway is more likely to occur on Cu-based catalysts with single atom doping and no by-product formation.

Conflicts of interest

There are no conflicts to declare.

Acknowledgements

The authors greatly appreciate Prof. B. J. Wang (Key Laboratory of Coal Science and Technology of Ministry of Education and Shanxi Province, Taiyuan University of Technology), who help us get access to the software of Materials Studio. In addition, the authors greatly appreciate the following financial supports: National Natural Science Foundation of China (No. 21706203), Scientific Research Program Funded by Shaanxi Provincial Education Department (No. 20JS161), PhD Research Startup Foundation of Yulin University (No. 18GK21 and 20GK01), the Key Research and Development Program of Shaanxi Province (No. 2020QFY05-04), Scientific Research Program of Yulin City (No. CXY-2020-002-01), Science and Technology Project of Shaanxi Administration for Market Regulation (No. 2021KY21), Key Laboratory of Energy Chemical Process Intensification (No. SXECPI201703).

References

- 1 A. Jangam, S. Das, N. Dewangan, P. Hongmanorom, W. M. Hui and S. Kawi, Conversion of CO₂ to C1 chemicals: Catalyst design, kinetics and mechanism aspects of the reactions, *Catal. Today*, 2020, **358**, 3–29.
- 2 T. A. Atsbha, T. Yoon, P. Seongho and C. J. Lee, A review on the catalytic conversion of CO₂ using H₂ for synthesis of CO, methanol, and hydrocarbons, *J. CO₂ Util.*, 2021, **44**, 101413.
- 3 S. Chakraborty, J. Nayak, B. Ruj, P. Pal and P. Chakraborty, Photocatalytic Conversion of CO₂ to Methanol using Membrane-Integrated Green Approach: A Review on Capture, Conversion and Purification, *J. Environ. Chem. Eng.*, 2020, **8**, 103935.
- 4 P. S. Murthy, W. Liang, Y. Jiang and J. Huang, Cu-Based Nanocatalysts for CO₂ Hydrogenation to Methanol, *Energ. Fuel.*, 2021, **35**, 8558–8584.
- 5 I. Tezsevin, S. Senkan, I. Onal and D. Düzenli, DFT Study on the Hydrogenation of CO₂ to Methanol on Ho-Doped Cu(211) Surface, *J. Phys. Chem. C*, 2020, **124**, 22426–22434.
- 6 K. F. Wei and M. Tahir, Recent trends in developments of active metals and heterogenous materials for catalytic CO₂ hydrogenation to renewable methane: a review, *J. Environ. Chem. Eng.*, 2021, **9**, 105460.
- 7 C. A. Qiao, A. Ym, A. Bq, A. Tz, B. Lw, A. Js and A. Xl, Z-scheme Bi/AgBiS₂/P25 for enhanced CO₂ photoreduction

- to CH₄ and CO with photo-thermal synergy, *Appl. Surf. Sci.*, 2021, **555**, 149648.
- 8 X. An, S. Li, X. Hao, Z. Xie and G. Guan, Common strategies for improving the performances of tin and bismuth-based catalysts in the electrocatalytic reduction of CO₂ to formic acid/formate, *Renewable Sustainable Energy Rev.*, 2021, **143**, 110952.
 - 9 Z. Ma, U. LeGrand, E. Pahija, J. R. Tavares and D. C. Boffito, From CO₂ to Formic Acid Fuel Cells, *Ind. Eng. Chem. Res.*, 2020, **60**, 803–815.
 - 10 S. Li, S. Sun, W. Suo, G. Liu, G. Wang, Y. Wang, J. Li and Z. Zhang, Theoretical investigation of electrochemical reduction mechanism of CO₂ on the Cu(111), Sn@Cu(111) and Sn(211) surfaces, *Appl. Surf. Sci.*, 2021, **564**, 150418.
 - 11 W. Gao, S. Liang, R. Wang, Q. Jiang, Y. Zhang, Q. Zheng, B. Xie, C. Y. Toe, X. Zhu, J. Wang, L. Huang, Y. Gao, Z. Wang, C. Jo, Q. Wang, L. Wang, Y. Liu, B. Louis, J. Scott, A.-C. Roger, R. Amal, H. He and S.-E. Park, Industrial carbon dioxide capture and utilization: state of the art and future challenges, *Chem. Soc. Rev.*, 2020, **49**, 8584–8686.
 - 12 A. Atakan, P. Mäkie, F. Söderlind, J. Keraudy, E. M. Björk and M. Odén, Synthesis of a Cu-infiltrated Zr-doped SBA-15 catalyst for CO₂ hydrogenation into methanol and dimethyl ether, *Phys. Chem. Chem. Phys.*, 2017, **19**, 19139–19149.
 - 13 D. Xu, Y. Wang, M. Ding, X. Hong, G. Liu and S. C. E. Tsang, Advances in higher alcohol synthesis from CO₂ hydrogenation, *Chem*, 2021, **7**, 849–881.
 - 14 S. Guo, J. Di, C. Chen, C. Zhu and Z. Liu, Oxygen Vacancy Mediated Bismuth Stannate Ultra-Small Nanoparticle towards Photocatalytic CO₂-to-CO Conversion, *Appl. Catal., B*, 2020, **276**, 119156.
 - 15 S. De, A. Dokania, A. Ramirez and J. Gascon, Advances in the design of heterogeneous catalysts and thermocatalytic processes for CO₂ utilization, *ACS Catal.*, 2020, **10**, 14147–14185.
 - 16 L. Ou, H. Yang, J. Jin and Y. Chen, Theoretical insights into the promotion effect of alkali metal cations on the electro-reduction mechanism of CO₂ into C1 products at the Cu(111)/H₂O interface, *New J. Chem.*, 2021, **45**, 15582–15593.
 - 17 Y. Liu, P. R. Murthy, X. Zhang, H. Wang and C. Shi, Phase transformation of iron oxide to carbide and Fe₃C as an active center for the RWGS reaction, *New J. Chem.*, 2021, **45**, 22444–22449.
 - 18 J. Wei, R. Yao, Y. Han, Q. Ge and J. Sun, Towards the development of the emerging process of CO₂ heterogenous hydrogenation into high-value unsaturated heavy hydrocarbons, *Chem. Soc. Rev.*, 2021, **45**, 10764–10805.
 - 19 X. Zhang, C. Liu, Y. Zhao, L. Li, Y. Chen, F. Raziq, L. Qiao, S.-X. Guo, C. Wang and G. G. Wallace, Atomic nickel cluster decorated defect-rich copper for enhanced C2 product selectivity in electrocatalytic CO₂ reduction, *Appl. Catal., B*, 2021, **291**, 120030.
 - 20 A. Mustafa, B. G. Lougou, Y. Shuai, Z. Wang and H. Tan, Current technology development for CO₂ utilization into solar fuels and chemicals: a review, *J. Energy Chem.*, 2020, **49**, 96–123.
 - 21 J. Hao, D. Yang, J. Wu, B. Ni, L. Wei, Q. Xu, Y. Min and H. Li, Utilizing new metal phase nanocomposites deep photocatalytic conversion of CO₂ to C₂H₄, *Chem. Eng. J.*, 2021, **423**, 130190.
 - 22 D. Karapinar, C. E. Creissen, J. G. Rivera de la Cruz, M. W. Schreiber and M. Fontecave, Electrochemical CO₂ Reduction to Ethanol with Copper-Based Catalysts, *ACS Energy Lett.*, 2021, **6**, 694–706.
 - 23 W. Wang, C. Deng, S. Xie, Y. Li, W. Zhang, H. Sheng, C. Chen and J. Zhao, Photocatalytic C-C Coupling from Carbon Dioxide Reduction on Copper Oxide with Mixed-Valence Copper(I)/Copper(II), *J. Am. Chem. Soc.*, 2021, **143**, 2984–2993.
 - 24 X. Wang, P. J. Ramirez, W. Liao, J. A. Rodriguez and P. Liu, Cesium-Induced Active Sites for C-C Coupling and Ethanol Synthesis from CO₂ Hydrogenation on Cu/ZnO (000 $\bar{1}$) Surfaces, *J. Am. Chem. Soc.*, 2021, **143**, 13103–13112.
 - 25 X. Gao and W. Yang, Reaction: key issues of solar-driven CO₂ conversion to fuel, *Chem*, 2020, **6**, 1041–1042.
 - 26 J. Yoshihara, S. Parker, A. Schafer and C. T. Campbell, Methanol synthesis and reverse water-gas shift kinetics over clean polycrystalline copper, *Catal. Lett.*, 1995, **31**, 313–324.
 - 27 Y. Yang, J. Evans, J. A. Rodriguez, M. G. White and P. Liu, Fundamental studies of methanol synthesis from CO₂ hydrogenation on Cu(111), Cu clusters, and Cu/ZnO (000 $\bar{1}$), *Phys. Chem. Chem. Phys.*, 2010, **12**, 9909–9917.
 - 28 Y. Yang, M. G. White and P. Liu, Theoretical study of methanol synthesis from CO₂ hydrogenation on metal-doped Cu(111) surfaces, *J. Phys. Chem. C*, 2012, **116**, 248–256.
 - 29 L. Grabow and M. Mavrikakis, Mechanism of methanol synthesis on Cu through CO₂ and CO hydrogenation, *ACS Catal.*, 2011, **1**, 365–384.
 - 30 S. Kattel, B. Yan, Y. Yang, J. G. Chen and P. Liu, Optimizing binding energies of key intermediates for CO₂ hydrogenation to methanol over oxide-supported copper, *J. Am. Chem. Soc.*, 2016, **138**, 12440–12450.
 - 31 K. Larmier, W. C. Liao, S. Tada, E. Lam, R. Verel, A. Bansode, A. Urakawa, A. Comas-Vives and C. Copéret, CO₂-to-methanol hydrogenation on zirconia-supported copper nanoparticles: reaction intermediates and the role of the metal-support interface, *Angew. Chem., Int. Ed.*, 2017, **56**, 2318–2323.
 - 32 N. Austin, J. Ye and G. Mpourmpakis, CO₂ activation on Cu-based Zr-decorated nanoparticles, *Catal. Sci. Technol.*, 2017, **7**, 2245–2251.
 - 33 H. Li, Y. Shen, H. Du, J. Li, H. Zhang and C. Xu, Insight into the mechanisms of CO₂ reduction to CHO over Zr-doped Cu nanoparticle, *Chem. Phys.*, 2021, **540**, 111012.
 - 34 Megha, K. Mondal, T. K. Ghanty and A. Banerjee, Adsorption and Activation of CO₂ on Small-Sized Cu-Zr Bimetallic Clusters, *J. Phys. Chem. A*, 2021, **125**, 2558–2572.
 - 35 B. Delley, An all-electron numerical method for solving the local density functional for polyatomic molecules, *J. Chem. Phys.*, 1990, **92**, 508–517.
 - 36 B. Delley, From molecules to solids with the DMol3 approach, *J. Chem. Phys.*, 2000, **113**, 7756–7764.
 - 37 A. Bergner, M. Dolg, W. Küchle, H. Stoll and H. Preuß, *Ab initio* energy-adjusted pseudopotentials for elements of groups 13–17, *Mol. Phys.*, 1993, **80**, 1431–1441.

- 38 J. P. Perdew, K. Burke and M. Ernzerhof, Generalized gradient approximation made simple, *Phys. Rev. Lett.*, 1996, **77**, 3865.
- 39 J. P. Perdew and Y. Wang, Accurate and simple analytic representation of the electron-gas correlation energy, *Phys. Rev. B: Condens. Matter Mater. Phys.*, 1992, **45**, 13244.
- 40 H. J. Monkhorst and J. D. Pack, Special points for Brillouin-zone integrations, *Phys. Rev. B: Condens. Matter Mater. Phys.*, 1976, **13**, 5188.
- 41 T. A. Halgren and W. N. Lipscomb, The synchronous-transit method for determining reaction pathways and locating molecular transition states, *Chem. Phys. Lett.*, 1977, **49**, 225–232.
- 42 J. Dean, Y. Yang, N. Austin, G. Vesper and G. Mpourmpakis, Design of copper-based bimetallic nanoparticles for carbon dioxide adsorption and activation, *ChemSusChem*, 2018, **11**, 1169–1178.
- 43 D. R. Lide, G. Baysinger and L. I. Berger *CRC Handbook of Chemistry and Physics*, 87th edn, CRC Press, Inc, 2007.
- 44 H.-J. Freund and M. W. Roberts, Surface chemistry of carbon dioxide, *Surf. Sci. Rep.*, 1996, **25**, 225–273.
- 45 C.-T. Yang, B. C. Wood, V. R. Bhethanabotla and B. Joseph, CO₂ adsorption on anatase TiO₂ (101) surfaces in the presence of subnanometer Ag/Pt clusters: implications for CO₂ photoreduction, *J. Phys. Chem. C*, 2014, **118**, 26236–26248.
- 46 E. E. Benson, C. P. Kubiak, A. J. Sathrum and J. M. Smieja, Electrocatalytic and homogeneous approaches to conversion of CO₂ to liquid fuels, *Chem. Soc. Rev.*, 2009, **38**, 89–99.
- 47 L. Liu, X. Su, H. Zhang, N. Gao, F. Xue, Y. Ma, Z. Jiang and T. Fang, Zirconia-modified copper catalyst for CO₂ conversion to methanol from DFT study, *Appl. Surf. Sci.*, 2020, **528**, 146900.
- 48 Q.-L. Tang, Q.-J. Hong and Z.-P. Liu, CO₂ fixation into methanol at Cu/ZrO₂ interface from first principles kinetic monte carlo, *J. Catal.*, 2009, **263**, 114–122.
- 49 L. Liu, F. Fan, Z. Jiang, X. Gao, J. Wei and T. Fang, Mechanistic study of Pd–Cu bimetallic catalysts for methanol synthesis from CO₂ hydrogenation, *J. Phys. Chem. C*, 2017, **121**, 26287–26299.